HHS Public Access

Author manuscript

J Leukoc Biol. Author manuscript; available in PMC 2020 June 01.

Published in final edited form as:

J Leukoc Biol. 2019 June ; 105(6): 1099–1110. doi:10.1002/JLB.4HI0918-364RR.

Employing enzymatic treatment options for management of ocular biofilm-based infections

Abirami Kugadas[1], **Jennifer Geddes-McAlister**[2], **Emilia Guy**[1], **Antonio DiGiandomenico**[3], **David B. Sykes**[4], **Michael K. Mansour**[5], **Rossen Mirchev**[6], **Mihaela Gadjeva**[1,*]

[1]Department of Medicine, Division of Infectious Diseases, Brigham and Women's Hospital, Harvard Medical School, Boston, MA 02115

[2]Proteomics and Signal Transduction Department, Max Planck Institute of Biochemistry, Martinsried, Germany, 82152

[3]MedImmune, LLC, Gaithersburg, MD 20878

[4]Center for Regenerative Medicine, Massachusetts General Hospital, Boston, MA 02114

[5]Division of Infectious Diseases, Massachusetts General Hospital, Boston, MA 02114

[6]Biological Chemistry and Molecular Pharmacology, Harvard Medical School, Boston, MA02115

Abstract

Pseudomonas aeruginosa–induced corneal keratitis is a sight-threatening disease. The rise of antibiotic resistance among *P. aeruginosa* keratitis isolates makes treatment of this disease challenging, emphasizing the need for alternative therapeutic modalities. By comparing the responses to *P. aeruginosa* infection between an outbred mouse strain (Swiss Webster, SW) and a susceptible mouse strain (C57BL6/N), we found that the inherent neutrophil-killing abilities of these strains correlated with their susceptibility to infection. Namely, SW-derived neutrophils were significantly more efficient at killing *P. aeruginosa in vitro* than C57BL6/N-derived neutrophils. To interrogate whether the distinct neutrophil killing capacities were dependent on endogenous or exogenous factors, neutrophil progenitor cell lines were generated. The *in vitro* differentiated neutrophils from either SW or C57BL6/N progenitors retained the differential killing abilities, illustrating that endogenous factors conferred resistance. Consistently, quantitative LC-MS/MS analysis revealed strain-specific and infection-induced alterations of neutrophil proteomes. Among the distinctly elevated proteins in the SW-derived proteomes were -mannosidases, potentially associated with protection. Inhibition of α-mannosidases reduced neutrophil bactericidal functions *in vitro*. Conversely, topical application of α-mannosidases reduced bacterial biofilms and burden of infected corneas. Cumulatively, these data suggest novel therapeutic approaches to control bacterial biofilm assembly and improve bacterial clearance via enzymatic treatments.

[*]**Corresponding author:** Mihaela Gadjeva, PhD., Division of Infectious Disease, Brigham and Women's Hospital, 181 Longwood Ave, Boston, MA 02115., tel 1-617-525-2268; fax 1-617-525-2510; mgadjeva@rics.bwh.harvard.edu.

Author Contributions Statement

AK, RM, EG, MG performed experiments and analyzed data. JG generated and analyzed the LC-MS data. DS and MM provided insight and helped generating PMN cell lines. AD provided the anti-psl MoAb. MG conceptualized the study, analyzed data, and wrote the manuscript. All authors critically read the manuscript.

Conflict of Interest

AD has interests in developing anti-Psl-MoAb-based therapies.

Graphical Abstract

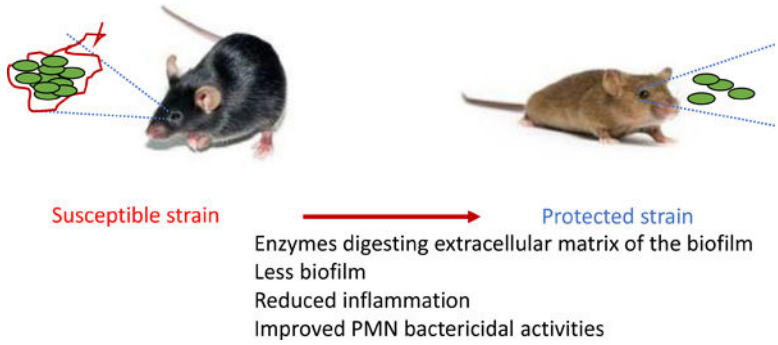

Summary sentence:

This article demonstrates the impact of alpha mannosidase for neutrophil handling of *P. aeruginosa* biofilms.

Keywords

innate immunity; neutrophils; *P. aeruginosa*; biofilms

Introduction

Eye trauma and contact lens use are the main factors that predispose to the development of infectious keratitis associated with vision loss and blindness [1; 2]. In the USA, 1 in 2,500 daily contact wearers and 1 in 500 overnight lens wearers develop bacterial keratitis, which constitutes a significant health problem. The organism that is most often isolated from contact lens–associated corneal ulcers is *Pseudomonas aeruginosa* [3; 4]. Existing therapies often fail to eradicate *P. aeruginosa* efficiently due to pathoadaptation and acquired antibiotic resistance, marking the need to find alternative therapeutic approaches [5]. Therefore, there is a significant interest in developing strategies to strengthen host resistance to infection.

The effective control and clearance of *P. aeruginosa* depends on engulfment, phagocytosis, and degradation of bacteria in a complex and highly regulated process that works in concert with other innate immune responses, such as inflammatory signals. Genetic deficiencies that compromise phagocytosis, reactive oxygen species (ROS) production, and phagocyte trafficking and adhesion result in a significant predisposition to infection [6]. In addition, bacteria harbor versatile mechanisms to reduce phagocyte functionality. For example, *P. aeruginosa* alters the dynamics of cytoskeletal changes associated with phagocytosis, blocks ROS synthesis and escapes phagocytic vacuoles via effectors released by the Type III secretion system [7; 8; 9; 10].

While *P. aeruginosa* can proliferate in the cytosol of phagocytic cells [11; 12], the majority of it is present extracellularly. During chronic infection, *P. aeruginosa* forms biofilms at mucosal sites, where it resides in a non-motile and protected from phagocytosis state. In biofilms, bacteria increase the synthesis of extracellular polysaccharides (EPS) to generate

biomatrix in which the individual bacterial cells are embedded. Three different types of polysaccharides—Psl, Pel, and alginate—have been described as essential to biofilm formation [13; 14; 15; 16; 17; 18; 19; 20]. Importantly, the different polysaccharides demonstrate distinct production kinetics, suggesting differential impact on the biofilm growth [21]. Whether *P. aeruginosa* forms biofilms during acute infections such as ocular keratitis remains controversial [22].

Interestingly, in biofilms *P. aeruginosa* is surrounded by neutrophils, which fail to breach bacterial structures resulting in a limited host response [23]. It is proposed that the extracellular polysaccharide matrix that covers *P. aeruginosa* biofilms inhibits complement activation and neutrophil phagocytosis [24; 25] due to entrapped active enzymes, such as ecotin, a Psl-binding protein with serine protease inhibitory that may inhibit complement convertase activation. Here, we describe a mechanism of biofilm decomposition activated in neutrophils derived from a strain of mice resistant to keratitis. We show that the production of polysaccharide degrading enzymes, including α-mannosidases, is elevated leading to more efficient biofilm breakdown. We propose that the production of enzymes that solubilize biofilms is a novel mechanism for anti-bacterial protection. Our work suggests that these enzymes could harbor therapeutic potential for treatment of infectious diseases.

Materials and methods

Ethics Statement

All animal experiments were performed following National Institutes of Health guidelines for housing and care of laboratory animals and performed in accordance with institutional regulations after protocol review and approval by BWH IACUC committee and were consistent with the Association for Research in Vision and Ophthalmology guidelines for studies in animals (protocol 311).

Mice

Mice were housed and bred at the MCP Animal Care Facility. Swiss Webster (SW) and C57BL/6N mice were purchased from Taconic Farms. Seven to nine-week old mice were used throughout the experiments. We have not observed significant differences in the bacterial clearance of male and female mice to ocular *P. aeruginosa*–induced infection.

Bacterial strains and inocula

Invasive *P. aeruginosa* clinical isolate 6294-GFP and PAO1-GFP strain were used throughout the experiments. For the imaging experiments, *P. aeruginosa* strains and clinical isolates PAO1, and 6354 were electroporated with pCdrA-GFP (kindly provided by Prof. Tolker-Nielsen [26]) and selected on gentamicin (15 μg/ml). The bacterial strains were grown overnight at 37^0C on Tryptic Soy Broth (TSB) (Cardinal Health) agar plates supplemented with 5% sheep blood. Bacterial suspensions were prepared in saline solution and used for subsequent infection experiments.

Infection model

Infections were carried out as described previously [27]. Briefly, mice were anesthetized with intraperitoneal ketamine and xylazine injections. Three 5 mm scratches were made on the cornea with 25G needle tip and an inoculum of 1×10^5 cfu of *P. aeruginosa* was delivered in 5 μl onto the eye. Mice remained sedated for approximately 30 min. For evaluation of corneal pathology, daily scores were recorded by an observer unaware of the experimental conditions based on the following scoring system using a graded scale of 0 to 4 as follows: 0, eye macroscopically identical to the uninfected contra-lateral control eye; 1, faint opacity partially covering the pupil; 2, dense opacity covering the pupil; 3, dense opacity covering the entire anterior segment; and 4, perforation of the cornea, phthisis bulbi (shrinkage of the globe after inflammatory disease), or both. To determine corneal bacterial counts at 24h after infection, mice were sacrificed, the eyes were enucleated, and the corneas were dissected from the ocular surface. To quantify *P. aeruginosa* levels, corneas were suspended in PBS, 0.05% Triton X100, serially diluted and plated on *P. aeruginosa* selective McConkey agar plates.

Purification of PMNs and bactericidal assays

Murine bone marrow was flushed from both hind limbs with PBS supplemented with 2% fetal bovine serum and 1 mM EDTA. The cells were washed, erythrocytes in the cell pellet were lysed using the Mouse Erythrolysis Kit (R&D Systems) according to the manufacturer's instruction, and neutrophils were isolated using the EasySep Mouse Neutrophil Enrichment Kit (Vancouver, Canada**)**. Neutrophils were incubated with *P. aeruginosa* strain PA01 at an MOI of 100:1 for 90 min at 37°C on a rotator. Aliquots taken at time 0 and 90 min were serially diluted and plated on McConkey agar to determine numbers of live *P. aeruginosa*. Percentage of killing ability of neutrophils was calculated [28].

Neutrophil cell lines and treatments

SW and C57BL6/N neutrophil progenitor cell lines were established as described in [29]. Neutrophil progenitors were maintained in RPMI supplemented with 10% FBS, penicillin-streptomycin, stem cell factor (SCF), and beta estradiol. The SCF was supplied as conditioned media from a CHO cell line engineered to produce SCF. 2% conditioned media was used, equating to a SCF concentration of ~100 ng/ml. The beta-estradiol (Sigma) was dissolved in ethanol at 10 mM stock and used at a final concentration of 0.5 μM. To differentiate into granulocytes, beta-estradiol was omitted from the growth media, and cells were cultured in RPMI media supplemented with 20 ng/ml GCSF (BioLegend), 10% FBS, penicillin-streptomycin, and maintained for either 3 or 5 days before performing the killing experiments. Typically, 1.5×10^6 granulocytes were either treated with swainsonine (Tocris) at a final concentration of 1 μg/ml or vehicle control for 2–3 hrs at 37C 5% CO2 before adding or murine serum and *P. aeruginosa* 6294. The bactericidal assay was performed as described above.

Intravital imaging

To image EPS, fluorescently labelled 0.5 μg mAb to Psl Cam003 [30], alginate F429 [19] or control human IgG1 [19] were topically applied to the cornea for 15 min, ocular surface was

washed thrice with 15 μl of PBS before imaging. To visualize neutrophils, C57BL6/N mice were injected with 5 μg fluorescently labelled anti-Ly6G (with either Alexa 674 or APC) (Thermo Fisher Scientific) IV for 30 min to 1h before imaging [31]. Video was acquired with an upright Olympus FV1000 intravital microscope (Center Valley, PA). The microscope was equipped with a LumPlan 40x/0.8 numerical aperture (NA) 20x water immersion objective and digitally recorded with an Olympus DP71 charge-coupled device video camera and Olympus FluoView 1000 imaging software. Some experiments were carried out using the imaging system as described in [8]. Images and 3D reconstructions were carried out using Image J and Matlab. Areas covered with bacterial biofilms were calculated and compared across different time points of biofilm growth. Neutrophil meandering index was calculated per individual tracks derived from at least 30 individual neutrophils per separate imaging. Meandering index was calculated as a ratio of displacement per individual track length.

Sample preparation for LC-MS/MS analysis

PMNs from infected and baseline SW and C57BL6/N mice (in triplicate or quadruplicate) were subjected to in-solution trypsin digestion. Briefly, 200 μl of 8 M Urea containing 40 mM HEPES was added to baseline and infected SW and C57BL6/N samples were sonicated in a rotating water bath at 4°C for 15 min (30 s on, 30 s off). The samples were then reduced with 10 mM dithiothreitol (DTT), alkylated with 55 mM iodoacetamide (IAA), followed by dilution with 50 mM ammonium bicarbonate to 2 M urea, and LysC and trypsin (protein: enzyme ratio 50:1) digestion overnight. Digestion was stopped by addition of 10% v/v trifluoroacetic acid (TFA) per sample and the acidified peptides were loaded onto StageTips (containing three layers of C_{18}) to desalt and purify according to the standard protocol [32]. Each sample was divided onto two StageTips (one “working” and one “back-up”) and stored at 4 °C until the LC-MS/MS measurement.

LC MS/MS measurement

Samples were eluted from StageTips with 50 μl buffer B (80% acetonitrile (ACN) and 0.5% acetic acid), the organic solvent was removed in a SpeedVac concentrator for 20 min, and peptides were resuspended in 10 μl of Buffer A (2% ACN and 0.1% TFA). 3 μl of each sample was analyzed by nanoflow liquid chromatography on an EASY-nLC system (Thermo Fisher Scientific, Bremen, Germany) on-line coupled to an Q Exactive HF-X quadrupole orbitrap mass spectrometer (Thermo Fisher Scientific) through a nanoelectrospray ion source (Thermo Fisher Scientific). A 50 cm column with 75 μm inner diameter was used for the chromatography, in-house packed with 3 μm reversed-phase silica beads (ReproSil-Pur C_{18}-AQ, Dr. Maisch GmbH, Germany). Peptides were separated and directly electrosprayed into the mass spectrometer using a linear gradient from 5% to 60% ACN in 0.5% acetic acid over 120 min at a constant flow of 300 nl/min. The linear gradient was followed by a washout with up to 95% ACN to clean the column for the next run. The overall gradient length was 145 min. The QExactive HF-X was operated in a data-dependent mode, switching automatically between one full-scan and subsequent MS/MS scans of the fifteen most abundant peaks (Top15 method), with full-scans (m/z 300–1650) acquired in the Orbitrap analyzer with a resolution of 60,000 at 100 m/z.

Raw Data processing

Raw files were analyzed together using MaxQuant software (version 1.5.6.2) [33]. The derived peak list was searched with the built-in Andromeda search engine [34; 35]against the reference *Mus musculus* proteome downloaded from Uniprot (http://www.uniprot.org/) (April 27, 2016; 53,106 sequences). The parameters were as follows: strict trypsin specificity was required with cleavage at the C-terminal after K or R, allowing for up to two missed cleavages. The minimum required peptide length was set to seven amino acids. Carbamidomethylation of cysteine was set as a fixed modification (57.021464 Da) and N-acetylation of proteins N termini (42.010565 Da) and oxidation of methionine (15.994915 Da) were set as variable modifications. PSM and protein identifications were filtered using a target-decoy approach at a false discovery rate (FDR) of 1%. 'Match between runs' was enabled with a match time window of 0.7 min and an alignment time window of 20 min. Relative, label-free quantification of proteins was done using the MaxLFQ algorithm [35] integrated into MaxQuant using a minimum ratio count of 2, enabled FastLFQ option, LFQ minimum number of neighbors at 3, and the LFQ average number of neighbors at 6. The mass spectrometry proteomics data have been deposited in the PRIDE partner repository for the ProteomeXchange Consortium with the data set identifier: PXD009767.

Data analysis

Further analysis of the MaxQuant-processed data was performed using the Perseus software environment (version 1.5.5.5) [36]. The "proteingroups.txt" file was loaded into Perseus. Hits to the reverse database, contaminants, and proteins only identified with modified peptides were eliminated. LFQ intensities were converted to a log scale (log2), and only those proteins which were present in triplicate within at least one sample set were used for further statistical analysis (valid-value filter of 3 in at least one group). Missing values were imputed from a normal distribution (downshift of 1.8 standard deviations and a width of 0.3 standard deviations). The total matrix was imputed using these values, enabling statistical analysis. A Welch's *t*-test was performed to identify proteins with a significant differential expression (*p-value* < 0.05) between baseline and infected SW and C57BL6/N (S0 = 1) samples employing a 5% permutation-based FDR filter. A Principle Component Analysis (PCA) was performed to determine proteome differences at the experiment level, as well as Pearson correlation with hierarchical clustering by Euclidean distance to determine replicate reproducibility. A two-sample Student's *t-test* (S0 =1) was performed on the entire data set and a 1D-annotation enrichment based on the *t-test* differences with a Benjamini-Hochberg FDR cutoff at 0.05 allowed for visualization of enrichment by keywords within the RStudio platform (http://www.R-project.org/). Specifically, annotation enrichment categories meeting the *p-value* (0.05) and FDR (0.05) cut-offs, along with scores < −0.5 and < 0.5 were plotted.

In vitro biofilm assays

Single colony of *P. aeruginosa 6294* was transferred to 3 ml of LB media and grown overnight to OD_{650}= 1.9 to 2.1. The overnight culture was diluted to OD_{650} = 0.5 with M63 media and seeded into 96-well plates for either 12h at 37°C. Wells were emptied, washed with PBS, and 125ul of 0.5% crystal violet solution added into each well. After 15 minutes incubation, plates were washed 3 times by submerging into distilled water and blotting

vigorously on paper towel. Plates were dried overnight and 125ul of 30% acetic acid added into each well to solubilize the crystal. Biofilms were quantified at 600 nm.

Mannosidase treatments

C57BL6/N mice were infected with 1–5 × 10^5 cfu of *P. aeruginosa 6294* delivered in 5 μl onto the eye as described above. Alpha mannosidase (New England Biolabs) (0.2 U/cornea) were applied topically every 3h after the infectious challenge for the duration of 12h. Mice were rested for 12h and infected corneas harvested at 24h post-infectious challenge. The control group received topical aliquots of mannosidase buffer.

Monoclonal antibody treatments

C57BL6/N mice were infected as described above with *P. aeruginosa 6294* delivered in 5 μl onto the eye as described above. 400 μg of anti-Psl mAb Cam 003[30] or isotype control Ab were applied topically every 6h after the infectious challenge for the duration of 24h.

Statistical analysis

Statistical analysis of corneal pathology scores, bacterial burden, and cytokine levels were either by Unpaired Student's *t*-test upon normal distribution, Mann-Whitney U test for pair-wise comparisons, or One-way ANOVA with Dunn's correction for Multigroup comparisons (Prism 4.0 for Macintosh. The analysis of the data from the bactericidal activity assays was based on the use of Unpaired Student's *t*-test or One-way ANOVA as appropriate. Differences were considered significant if the p value was <0.05 (Prism 4.0 for Macintosh).

Results

Neutrophils fail to penetrate Psl-containing *P. aeruginosa* biofilms at ocular surfaces

Biofilms are defined as clusters of bacteria encapsulated in EPS. Intravital detection of biofilms during keratitis has been challenging because of a lack of EPS-specific reagents. Recent investigation based on cryo-electron microscopy imaging showed that *P. aeruginosa* formed bacterial microclusters on ocular surfaces, consistent with biofilm formation, but the nature of the EPS was not explored [22]. Using intravital imaging, we monitored *P. aeruginosa* PAO1 expressing CdrA-driven GFP behavior during infection [26]. This was combined with analysis of the EPS composition by use of fluorescently-labelled anti-Psl mAb Cam 003 that specifically recognizes Psl [30]. During the early stages of infection, bacteria formed individual bacterial clusters or microcolonies likely emanating from infected epithelial cells (early biofilms) (Fig. 1A), whereas at later time points biofilms were observed where bacteria resided in sheets (late biofilms) (Fig. 1A). Expectedly, bacterial biofilms grew in size during infection (Fig. 1A). The biofilms were surrounded with Psl (Fig. 1C). In contrast to Psl, low abundance of alginate presence was detected (data not shown) and the alginate-deficient clinical *P. aeruginosa* isolate 6354 formed biofilms at ocular surfaces (data not shown), indicative that alginate presence was not required for ocular biofilm formation. Cumulatively, these data suggest that Psl is a dominant polysaccharide among the ones tested making it a rational target for treatment.

We utilized intravital imaging to directly monitor *P. aeruginosa* behavior during ocular infection (Fig. 2, S1) and found that bacterial biofilms were protected from neutrophil infiltration (Fig. 2, S1 and S2). PMNs approached bacterial biofilms in swarms (Fig.2 A, top right corner, S1). Individual PMNs were visible at the border of the biofilms (Fig2A, yellow line) where they showed decreased motilities when compared to the motilities of neutrophils within the swarm or at sites where planktonic bacteria were visible (S1). Neutrophils probed biofilms by extending phyllopodia against bacterial biofilms, but could not easily penetrate biofilms (S2). These data suggest that intervention strategies to disrupt biofilms could improve neutrophil function by permitting access to bacteria themselves.

mAbs against Psl improves opsonophagocytosis *in vitro* but shows no therapeutic efficacy *in vivo*

The use of Psl-specific mAbs was previously reported to demonstrate good prophylactic efficacy in a lung and keratitis infection models after systemic administration [30]. Here, we evaluated the opsonophagocytic killing (OPK) activity of anti-Psl mAb Cam003 against keratitis isolates, examined its bactericidal efficacy against *P. aeruginosa* grown in a planktonic and micro-aggregated forms, and its therapeutic ability *in vivo*. Consistent with previous data the anti-Psl mAb Cam003 showed significant OPK activity against keratitis clinical *P. aeruginosa* isolates 6294, 6354, and laboratory strain PAO1 (data not shown) [30]. Notably, the OPK activity was diminished when *P. aeruginosa* was grown in the presence of eukaryotic cells to allow micro-aggregate formation (Fig. 3A). However, despite these prominent *in vitro* effects, the topical application of Cam003 at 6 hours following the infectious challenge was not sufficient to diminish the bacterial corneal burden and the accompanying inflammation (Fig. 3B and 3C). No changes in neutrophil influx were observed, as measured by corneal neutrophil elastase levels or by neutrophil attracting cytokines IL-1β and MIP-2 (Fig. 3C).

SW mice are resistant to *P. aeruginosa* keratitis

To identify modalities that may promote efficient bacterial clearance, we examined immune responses to *P. aeruginosa*–induced keratitis in Swiss Webster (SW) and C57BL6/N mice. Unlike the C57BL6/N mice, the SW mice appeared resistant to infection and cleared *P. aeruginosa* (Fig. 4A). This correlated with the *ex vivo* ability of SW-derived neutrophils to kill *P. aeruginosa* more efficiently than the C57BL/6N-derived neutrophils (Fig. 4B).

To identify potential molecular mechanisms responsible for the improved bactericidal activity of SW-derived neutrophils, quantitative proteomic analysis was performed on neutrophils derived from non-infected (baseline) and *P. aeruginosa*–infected SW and C57BL6/N mice. In total, 4,297 proteins were identified from triplicate samples of SW baseline, SW infected, C57BL6/N baseline, and C57BL6/N infected cells. Biological replicate reproducibility ranged from 92% to 95%. A Principle Component Analysis (PCA) demonstrated clear clustering of the biological replicates (Fig. 5A) and distinct patterns of protein responses among the strains and treatments (component 1 at 37.2%; component 2 at 16.3%), illustrating active remodeling of the proteomes in the neutrophils derived from the infected mice. The volcano plots compare the differentially present proteins across genotypes (SW versus C57BL6/N). We identified 366 proteins with significant differences

in abundance upon comparison of PMN proteomes (Fig. 5B). Additionally, we identified 695 proteins with significant differences in abundance upon comparison of PMN proteomes derived from infected SW and C57BL6/N mice (Fig. 5C).

Interestingly, 1D annotation enrichment profiling based on keywords of the significantly different neutrophil proteins (*p-value* < 0.05; FDR < 0.05) identified among the comparisons, revealed patterns of enrichment between the proteomes of neutrophils derived from infected C57BL6/N mice versus non-infected C57BL6/N mice (Fig. 5D comparison 1) and between the proteomes of neutrophils derived from the infected C57BL6/N and infected SW mice (Fig. 5D. comparison 4). These results suggest clear differences in neutrophil responses during infection in the C57BL6/N strain, as well as differential neutrophil outcomes between the mouse strains. Namely, neutrophil responses to infection included proteins associated with translocation, splicesome formation, regulation of mRNA splicing, mRNA processing, RNA-binding, and methylation. Positive enrichment of membrane-associated proteins was also observed including transmembrane proteins, transmembrane helix proteins, and mitochondrion inner membrane proteins, which suggests that processes of cellular remodeling are involved. Finally, secreted proteins and proteins of the endoplasmic reticulum were positively enriched, indicating secretory pathway involvement as a response to infection, which may be a potential connection with the observed alpha mannosidase activity and secretion. Similarities in lower-limit enrichment was observed for enzymatic processes (e.g. ligase, serine/threonine-protein kinase, GTPase activation, and Ubl conjugation), cellular compartments (e.g. cytoplasm), and general cellular processes (e.g. ATP-binding), suggesting reduced involvement during infection. Conversely, strain-specific differences in neutrophil responses through positive enrichment showed differential responses of lectin and calcium-associated pathways, indicating changes in cellular processes and metabolism. Additionally, differences in lower-limit enrichment included differences in kinase, hydrolase, transferase, and nucleotide-binding categories, associated with post-translational modifications and cellular regulation.

Only two categories of proteins stood out when comparing the1D annotation enrichment keyword profiling between infected SW versus baseline SW (Fig. 5D - 2) and baseline C57BL6/N versus baseline SW (Fig. 5D–3) proteomes. These included responses associated with post-translational modifications by acetylation which are typically involved in cell signaling, thereby enabling differential cellular reactions to perturbations, suggestive of infection-associated and strain-specific responses (Fig. 5D). Conversely, chaperone-associated proteins were positively enriched in a strain-specific manner, indicating changes in protein folding and cellular stress response. Taken together, these results demonstrated clear differences in protein enrichment profiles between baseline and infection, as well as strain-specific responses, which likely contributed to the overall observations of differential neutrophil killing abilities between the mice strains.

Specifically, the abundance of lysosomal proteins with enzymatic activities were of particular interest due to differential patterns of regulation in the SW-derived PMNs at baseline and during infection. Namely, chitotriosidase-1 (Chit1) showed a 5.9- and 5.3-fold increase in abundance at baseline and during infection, respectively, as compared to C57BL/6N-derived proteomes; cathepsin E (CtsE) showed a 4.0- fold increase in abundance

at baseline and during infection, respectively, as compared to the proteomes from C57BL/6N-derived neutrophils. Lysosomal alpha mannosidase (Man2b1) showed a 5.0- and 2.9-fold increase in abundance at baseline and during infection, respectively, as compared to C57BL/6N neutrophils (Fig. 5B; 5C). Also of interest was alpha mannosidase (Man2c1) which showed a 5.4-fold increase in abundance in infected SW-derived neutrophils as compared to infected C57BL/6N-derived neutrophils, but was not significantly different at baseline (Fig. 5C). Cumulatively, these data suggested that SW-derived neutrophils are more capable of producing proteins with anti-inflammatory and antimicrobial activities than their C57BL/6N counterparts. Further, our data showed that infection altered neutrophil proteomes demonstrating that these cells were significantly more plastic than previously appreciated and suggestive that the changes fine tuned neutrophil responses to pathogens.

Neutrophil cell intrinsic characteristics govern their superior bactericidal capacity against *P. aeruginosa*

To examine whether the differential killing of *P. aeruginosa* had cell-intrinsic component, neutrophil progenitor cell lines were developed from the bone marrow of both SW or C57BL6/N mice and allowed to mature *in vitro* to neutrophils (Fig. 6A). To verify that cell-intrinsic characteristics are responsible for differential killing of *P. aeruginosa*, SW-derived and C57BL/6N-derived neutrophil cell lines were matured with GCSF and their bactericidal capacities examined. Electron microscopy-based analysis of matured cells demonstrated appearance of cells with typical multilobed nuclei, characteristic to PMNs (Fig. 6A). Similar to the data generated with primary neutrophils, the *in vitro* SW-derived neutrophils were better at killing *P. aeruginosa* when compared to C57BL6/N-derived neutrophils (Fig. 6B, One-way ANOVA) even when exposed to GCSF priming.

To verify that the bactericidal activity of SW-derived neutrophils was dependent on α-mannosidases, GCSF-primed SW neutrophil cell line or bone marrow-derived primary neutrophils were pre-treated with the α-mannosidase inhibitor swainsonine and challenged with *P. aeruginosa* (Fig. 6C and D). In either of the comparisons, the SW neutrophil bactericidal activities were significantly reduced by swainsonine treatment (Fig. 6C, $p=0.007$, Student's *t*-test and Fig. 6D, $p=0.02$, Student's *t*-test), confirming the contribution of α−mannosidase in *P. aeruginosa* killing. Cumulatively, these data suggest that α-mannosidase facilitates bactericidal function of neutrophils.

Alpha mannosidase treatment reduces bacterial burden during keratitis

Given that Psl is a mannose-rich polysaccharide and that α-mannosidase digests [37], the biofilm-reducing capacity of exogenously-added α-mannosidase was examined. Bacterial biofilms of *P. aeruginosa* 6294 were grown for 24h and treated with α-mannosidase for 3h at 37°C after biofilms had formed. Mannosidase treatment significantly reduced biofilm density (Fig. 7A, Student's *t*-test, $p=0.006$). Further, a cyclic Di-GMP reporter PAO1 strain was allowed to form biofilms and was subsequently treated with α-mannosidase. The decrease in reporter-based fluorescence upon treatment accompanied the reduction in Psl-based biofilm formation (Fig. 7B, Student's *t*-test, $p=0.02$). Lastly, C57BL6/N mice were treated topically with α-mannosidase every 3h for 12h after the infectious challenge. Mice

receiving topical mannosidase exhibited reduced bacterial burden when compared to the placebo-treated mice (Student's *t*-test, p=0.008) (Fig. 7C).

Discussion

To date, the in-depth analysis of bacterial biofilms at ocular surfaces has been hindered by the lack of information about the nature of the bacterial polysaccharides in the matrix, lack of polysaccharide specific antibodies, imaging that requires tissue fixation and *ex vivo* analysis of corneas [22]. Using intravital imaging in live animals, we demonstrated that ocular *P. aeruginosa* biofilms are Psl-rich. Consequently, our data suggest a niche-specific adaptation of *P. aeruginosa*. Based on these observations we reason that treatment of ocular keratitis could be tailored to that niche.

While the majority of keratitis isolates produce Psl [18], we can not exclude contributions from other polysaccharides or matrix components in *P. aeruginosa* biofilms. For example, it is known that PA14 lacks Psl, is virulent in ocular keratitis models. Hence, it is likely that Psl is sufficient for *P. aeruginosa* pathoadaptation to the ocular niche, but not required.

Interestingly, the administration of the anti-Psl mAb was not sufficient to ameliorate keratitis, despite its excellent *in vitro* OPK characteristics. Indeed, we observed a two-fold increase in the recovered bacteria from the infected corneas of the mAb-treated group (Fig. 3). A possible explanation is lack of penetrance of neutrophils inside the biofilm even when biofilm were covered with anti-Psl- specific antibodies. Fewer neutrophils were present at the surface or close to the surface of the biofilms, while the majority of the neutrophils appeared under the biofilms, within the epithelial and/or stromal layer of the eye. Since Psl covered and surrounded bacterial biofilms at the ocular surface, the lack of therapeutic effect may be explained with the reduced neutrophil presence. Alternatively, defects in ability of neutrophils to digest biofilms even in the presence of polysaccharide-specific antibodies may contribute to the process, which would be consistent with the data presented here. Lastly, additional virulence factors may impair neutrophil functionality in the vicinity of biofilms. Given the recently-reported benefit of the bispecific anti-Psl and anti-PcrV antibody in multiple animal infection models [8; 38; 39], it is likely that targeting of the Type III secretion system is needed to confer protection.

To identify modalities that promote efficient bacterial clearance, we examined immune responses to *P. aeruginosa*–induced keratitis in Swiss Webster and C57BL6/N mice. Unlike the C57BL6/N mice, the SW mice appeared resistant to infection and cleared *P. aeruginosa in vivo*. This correlated with the ability of SW-derived neutrophils to kill *P. aeruginosa in vitro* more efficiently than C57BL/6N-derived neutrophils.

To identify potential mechanisms for improved bactericidal activity, we used quantitative LC-MS approach. We identified more than 4000 total proteins per neutrophil proteome, which exceeds significantly the pool of 2000 proteins reported in previous proteomic studies [40; 41; 42; 43]. Based on our proteomic data, we identified infection and strain-specific differences in the neutrophil proteomic networks.

For the purposes of this particular investigation we chose to focus on α-mannosidases that were significantly more abundant in the neutrophils derived from the SW mice, suggestive of their contribution to protective immunity. Because Psl is a polymer of pentameric repeating units of D-mannose, L-rhamnose, and D-glucose, where the individual α-D-mannose residues are connected with linkages, suitable for digest by the identified via LC-MS/MS α-mannosidases (e.g., Man2b1). We tested the importance of α-mannosidases in regulating biofilm formation and bactericidal properties of neutrophils. Consistent with recently published data by others [44], we observed that treatment with α-mannosidase *in vitro* decreased *P. aeruginosa* biofilms. Another recent study demonstrated that α-mannosidase targeted Psl [37]. Furthermore, Psl inhibited neutrophil bactericidal activity [37] and protected bacteria from proteolytic attach by neutrophil elastase [25]. We confirmed and expanded on this foundation by providing evidence that neutrophil-derived α-mannosidase activity is needed for optimal bactericidal function against *P. aeruginosa* and that the topical application of α-mannosidase decreased corneal bacterial burden *in vivo* at least initially during infection (Fig. 7). Cumulatively, these findings suggested that exogenous α-mannosidases alter Psl structure in such a way that render *P. aeruginosa* more susceptible to killing.

In humans, α-mannosidase is present in the lysosomes and is secreted extracellularly [45] [46]. Mutations that impair lysosomal α-mannosidase (Man2b1) activity cause development of α-mannosidosis, a condition that is rare, autosomal recessive, and multisystemic. This progressive lysosomal storage disorder results in facial and skeletal abnormalities, motor impairment, hearing impairment, intellectual disability, immune deficiency, and recurrent infections [47]. Importantly, the recombinant human α-mannosidase shows promise in clinical trials for enzyme replacement therapy [48]. The recombinant α-mannosidase is well-tolerated; the frequency of infusion-related reactions and the development of allo-antibodies are low compared to other enzyme replacement therapies [48]. These findings are exciting as they suggest that the use of recombinant human α-mannosidase for treatment of other conditions such as treatment of biofilm-based infections may be feasible and well-tolerated.

The pool of differentially expressed proteins also included additional proteins such as cathepsin E (4.7 fold), CD14 (2.5 fold), and chitotriosidase-1 (3.6 fold). Previous studies have documented that CD14 deficiency was associated with altered kinetics of *P. aeruginosa*–induced keratitis, implicating CD14-triggered pathways in promoting inflammation-induced corneal tissue damage in the C57BL/6 mice [49]. Consistently, chitotriosidase-1 deficiency altered inflammatory responses to *K. pneumoniae* in the infected lungs of C57BL6 mice, resulting in less pathology [50]. Lastly, overexpression of cathepsin E was associated with alterations in the kinetics of phagolysosomal assembly, terminating phagolysosomal maturation [51]. Cumulatively, these data illustrate that the infected SW-derived PMNs had proteomes that bear unique features, reflective of distinct neutrophil functions that were associated with improved recovery. It is of our current interest to find out how to leverage this knowledge therapeutically to promote resolution of infection.

Supplementary Material

Refer to Web version on PubMed Central for supplementary material.

Acknowledgements

Authors wish to thank Dr. Ajitha Thanabalasuriar and Prof. P. Kubes (University of Calgary, Canada) for providing expertise and help during the initial experiments of imaging of bacterial biofilms. We thank Maria Ericsson (Harvard Electron Microscopy (EM) core) for EM analysis.

Funding disclosure

This work was supported by NIH-NEI RO1 EY022054 to MG.

References

[1]. Robertson DM, Petroll WM, Jester JV, and Cavanagh HD, The role of contact lens type, oxygen transmission, and care-related solutions in mediating epithelial homeostasis and pseudomonas binding to corneal cells: an overview. Eye & contact lens 33 (2007) 394–8; discussion 399–400. [PubMed: 17975430]

[2]. Robertson DM, Petroll WM, Jester JV, and Cavanagh HD, Current concepts: contact lens related Pseudomonas keratitis. Cont Lens Anterior Eye 30 (2007) 94–107. [PubMed: 17084658]

[3]. Fleiszig SM, and Evans DJ, The pathogenesis of bacterial keratitis: studies with Pseudomonas aeruginosa. Clin Exp Optom 85 (2002) 271–8. [PubMed: 12366347]

[4]. Fleiszig SM, The Glenn A Fry award lecture 2005. The pathogenesis of contact lens-related keratitis. Optom Vis Sci 83 (2006) 866–73. [PubMed: 17164674]

[5]. O'Brien TP, Maguire MG, Fink NE, Alfonso E, and McDonnell P, Efficacy of ofloxacin vs cefazolin and tobramycin in the therapy for bacterial keratitis. Report from the Bacterial Keratitis Study Research Group. Archives of ophthalmology 113 (1995) 1257–65. [PubMed: 7575256]

[6]. Andrews T, and Sullivan KE, Infections in patients with inherited defects in phagocytic function. Clin Microbiol Rev 16 (2003) 597–621. [PubMed: 14557288]

[7]. Vareechon C, Zmina SE, Karmakar M, Pearlman E, and Rietsch A, Pseudomonas aeruginosa Effector ExoS Inhibits ROS Production in Human Neutrophils. Cell Host Microbe 21 (2017) 611–618 e5. [PubMed: 28494242]

[8]. Thanabalasuriar A, Surewaard BG, Willson ME, Neupane AS, Stover CK, Warrener P, Wilson G, Keller AE, Sellman BR, DiGiandomenico A, and Kubes P, Bispecific antibody targets multiple Pseudomonas aeruginosa evasion mechanisms in the lung vasculature. J Clin Invest 127 (2017) 2249–2261. [PubMed: 28463232]

[9]. Lovewell RR, Patankar YR, and Berwin B, Mechanisms of phagocytosis and host clearance of Pseudomonas aeruginosa. Am J Physiol Lung Cell Mol Physiol 306 (2014) L591–603. [PubMed: 24464809]

[10]. Fleiszig SM, Evans DJ, Do N, Vallas V, Shin S, and Mostov KE, Epithelial cell polarity affects susceptibility to Pseudomonas aeruginosa invasion and cytotoxicity. Infection and immunity 65 (1997) 2861–7. [PubMed: 9199460]

[11]. Fleiszig SM, Zaidi TS, Fletcher EL, Preston MJ, and Pier GB, Pseudomonas aeruginosa invades corneal epithelial cells during experimental infection. Infection and immunity 62 (1994) 3485–93. [PubMed: 8039920]

[12]. Fleiszig SM, Zaidi TS, and Pier GB, Pseudomonas aeruginosa invasion of and multiplication within corneal epithelial cells in vitro. Infection and immunity 63 (1995) 4072–7. [PubMed: 7558321]

[13]. Jennings LK, Storek KM, Ledvina HE, Coulon C, Marmont LS, Sadovskaya I, Secor PR, Tseng BS, Scian M, Filloux A, Wozniak DJ, Howell PL, and Parsek MR, Pel is a cationic exopolysaccharide that cross-links extracellular DNA in the Pseudomonas aeruginosa biofilm matrix. Proc Natl Acad Sci U S A 112 (2015) 11353–8. [PubMed: 26311845]

[14]. Parsek MR, Controlling the Connections of Cells to the Biofilm Matrix. Journal of bacteriology 198 (2016) 12–4. [PubMed: 26527642]

[15]. Ma L, Lu H, Sprinkle A, Parsek MR, and Wozniak DJ, Pseudomonas aeruginosa Psl is a galactose- and mannose-rich exopolysaccharide. Journal of bacteriology 189 (2007) 8353–6. [PubMed: 17631634]

[16]. Colvin KM, Irie Y, Tart CS, Urbano R, Whitney JC, Ryder C, Howell PL, Wozniak DJ, and Parsek MR, The Pel and Psl polysaccharides provide Pseudomonas aeruginosa structural redundancy within the biofilm matrix. Environmental microbiology 14 (2012) 1913–28. [PubMed: 22176658]

[17]. Zhao K, Tseng BS, Beckerman B, Jin F, Gibiansky ML, Harrison JJ, Luijten E, Parsek MR, and Wong GC, Psl trails guide exploration and microcolony formation in Pseudomonas aeruginosa biofilms. Nature 497 (2013) 388–91. [PubMed: 23657259]

[18]. Zegans ME, DiGiandomenico A, Ray K, Naimie A, Keller AE, Stover CK, Lalitha P, Srinivasan M, Acharya NR, and Lietman TM, Association of Biofilm Formation, Psl Exopolysaccharide Expression, and Clinical Outcomes in Pseudomonas aeruginosa Keratitis: Analysis of Isolates in the Steroids for Corneal Ulcers Trial. JAMA ophthalmology 134 (2016) 383–9. [PubMed: 26846404]

[19]. Zaidi T, and Pier GB, Prophylactic and therapeutic efficacy of a fully human immunoglobulin G1 monoclonal antibody to Pseudomonas aeruginosa alginate in murine keratitis infection. Infection and immunity 76 (2008) 4720–5. [PubMed: 18644881]

[20]. Ma L, Conover M, Lu H, Parsek MR, Bayles K, and Wozniak DJ, Assembly and development of the Pseudomonas aeruginosa biofilm matrix. PLoS pathogens 5 (2009) e1000354. [PubMed: 19325879]

[21]. Ghafoor A, Hay ID, and Rehm BH, Role of exopolysaccharides in Pseudomonas aeruginosa biofilm formation and architecture. Applied and environmental microbiology 77 (2011) 5238–46. [PubMed: 21666010]

[22]. Saraswathi P, and Beuerman RW, Corneal Biofilms: From Planktonic to Microcolony Formation in an Experimental Keratitis Infection with Pseudomonas Aeruginosa. The ocular surface 13 (2015) 331–45. [PubMed: 26220579]

[23]. Kragh KN, Alhede M, Jensen PO, Moser C, Scheike T, Jacobsen CS, Seier Poulsen S, Eickhardt-Sorensen SR, Trostrup H, Christoffersen L, Hougen HP, Rickelt LF, Kuhl M, Hoiby N, and Bjarnsholt T, Polymorphonuclear leukocytes restrict growth of Pseudomonas aeruginosa in the lungs of cystic fibrosis patients. Infection and immunity 82 (2014) 4477–86. [PubMed: 25114118]

[24]. Mishra M, Byrd MS, Sergeant S, Azad AK, Parsek MR, McPhail L, Schlesinger LS, and Wozniak DJ, Pseudomonas aeruginosa Psl polysaccharide reduces neutrophil phagocytosis and the oxidative response by limiting complement-mediated opsonization. Cellular microbiology 14 (2012) 95–106. [PubMed: 21951860]

[25]. Tseng BS, Reichhardt C, Merrihew GE, Araujo-Hernandez SA, Harrison JJ, MacCoss MJ, and Parsek MR, A Biofilm Matrix-Associated Protease Inhibitor Protects Pseudomonas aeruginosa from Proteolytic Attack. MBio 9 (2018).

[26]. Rybtke MT, Borlee BR, Murakami K, Irie Y, Hentzer M, Nielsen TE, Givskov M, Parsek MR, and Tolker-Nielsen T, Fluorescence-based reporter for gauging cyclic di-GMP levels in Pseudomonas aeruginosa. Applied and environmental microbiology 78 (2012) 5060–9. [PubMed: 22582064]

[27]. Preston MJ, Fleiszig SM, Zaidi TS, Goldberg JB, Shortridge VD, Vasil ML, and Pier GB, Rapid and sensitive method for evaluating Pseudomonas aeruginosa virulence factors during corneal infections in mice. Infect Immun 63 (1995) 3497–501. [PubMed: 7642283]

[28]. Dwyer M, and Gadjeva M, Opsonophagocytic assay. Methods Mol Biol 1100 (2014) 373–9. [PubMed: 24218277]

[29]. Odegaard JI, Vats D, Zhang L, Ricardo-Gonzalez R, Smith KL, Sykes DB, Kamps MP, and Chawla A, Quantitative expansion of ES cell-derived myeloid progenitors capable of differentiating into macrophages. J Leukoc Biol 81 (2007) 711–9. [PubMed: 17158607]

[30]. DiGiandomenico A, Warrener P, Hamilton M, Guillard S, Ravn P, Minter R, Camara MM, Venkatraman V, Macgill RS, Lin J, Wang Q, Keller AE, Bonnell JC, Tomich M, Jermutus L, McCarthy MP, Melnick DA, Suzich JA, and Stover CK, Identification of broadly protective human antibodies to Pseudomonas aeruginosa exopolysaccharide Psl by phenotypic screening. J Exp Med 209 (2012) 1273–87. [PubMed: 22734046]

[31]. Kolaczkowska E, Jenne CN, Surewaard BG, Thanabalasuriar A, Lee WY, Sanz MJ, Mowen K, Opdenakker G, and Kubes P, Molecular mechanisms of NET formation and degradation revealed by intravital imaging in the liver vasculature. Nature communications 6 (2015) 6673.

[32]. Rappsilber J, Mann M, and Ishihama Y, Protocol for micro-purification, enrichment, pre-fractionation and storage of peptides for proteomics using StageTips. Nat Protoc 2 (2007) 1896–906. [PubMed: 17703201]

[33]. Cox J, and Mann M, MaxQuant enables high peptide identification rates, individualized p.p.b.-range mass accuracies and proteome-wide protein quantification. Nat Biotechnol 26 (2008) 1367–72. [PubMed: 19029910]

[34]. Cox J, Neuhauser N, Michalski A, Scheltema RA, Olsen JV, and Mann M, Andromeda: a peptide search engine integrated into the MaxQuant environment. J Proteome Res 10 (2011) 1794–805. [PubMed: 21254760]

[35]. Cox J, Hein MY, Luber CA, Paron I, Nagaraj N, and Mann M, Accurate proteome-wide label-free quantification by delayed normalization and maximal peptide ratio extraction, termed MaxLFQ. Mol Cell Proteomics 13 (2014) 2513–26. [PubMed: 24942700]

[36]. Tyanova S, Temu T, Sinitcyn P, Carlson A, Hein MY, Geiger T, Mann M, and Cox J, The Perseus computational platform for comprehensive analysis of (prote)omics data. Nat Methods 13 (2016) 731–40. [PubMed: 27348712]

[37]. Hill PJ, Scordo JM, Arcos J, Kirkby SE, Wewers MD, Wozniak DJ, and Torrelles JB, Modifications of Pseudomonas aeruginosa cell envelope in the cystic fibrosis airway alters interactions with immune cells. Sci Rep 7 (2017) 4761. [PubMed: 28684799]

[38]. Le HN, Quetz JS, Tran VG, Le VTM, Aguiar-Alves F, Pinheiro MG, Cheng L, Yu L, Sellman BR, Stover CK, DiGiandomenico A, and Diep BA, MEDI3902 Correlates of Protection against Severe Pseudomonas aeruginosa Pneumonia in a Rabbit Acute Pneumonia Model. Antimicrobial agents and chemotherapy 62 (2018).

[39]. DiGiandomenico A, Keller AE, Gao C, Rainey GJ, Warrener P, Camara MM, Bonnell J, Fleming R, Bezabeh B, Dimasi N, Sellman BR, Hilliard J, Guenther CM, Datta V, Zhao W, Gao C, Yu XQ, Suzich JA, and Stover CK, A multifunctional bispecific antibody protects against Pseudomonas aeruginosa. Sci Transl Med 6 (2014) 262ra155.

[40]. Loi ALT, Hoonhorst S, van Aalst C, Langereis J, Kamp V, Sluis-Eising S, Ten Hacken N, Lammers JW, and Koenderman L, Proteomic profiling of peripheral blood neutrophils identifies two inflammatory phenotypes in stable COPD patients. Respir Res 18 (2017) 100. [PubMed: 28532454]

[41]. Tak T, Wijten P, Heeres M, Pickkers P, Scholten A, Heck AJR, Vrisekoop N, Leenen LP, Borghans JAM, Tesselaar K, and Koenderman L, Human CD62L(dim) neutrophils identified as a separate subset by proteome profiling and in vivo pulse-chase labeling. Blood 129 (2017) 3476–3485. [PubMed: 28515092]

[42]. McLeish KR, Merchant ML, Klein JB, and Ward RA, Technical note: proteomic approaches to fundamental questions about neutrophil biology. J Leukoc Biol 94 (2013) 683–92. [PubMed: 23470899]

[43]. Serwas NK, Huemer J, Dieckmann R, Mejstrikova E, Garncarz W, Litzman J, Hoeger B, Zapletal O, Janda A, Bennett KL, Kain R, Kerjaschky D, and Boztug K, CEBPE-Mutant Specific Granule Deficiency Correlates With Aberrant Granule Organization and Substantial Proteome Alterations in Neutrophils. Front Immunol 9 (2018) 588. [PubMed: 29651288]

[44]. Banar M, Emaneini M, Satarzadeh M, Abdellahi N, Beigverdi R, Leeuwen WB, and Jabalameli F, Evaluation of Mannosidase and Trypsin Enzymes Effects on Biofilm Production of Pseudomonas aeruginosa Isolated from Burn Wound Infections. PloS one 11 (2016) e0164622. [PubMed: 27736961]

[45]. Rose DR, Structure, mechanism and inhibition of Golgi alpha-mannosidase II. Current opinion in structural biology 22 (2012) 558–62. [PubMed: 22819743]

[46]. Tasegian A, Paciotti S, Ceccarini MR, Codini M, Moors T, Chiasserini D, Albi E, Winchester B, van de Berg WDJ, Parnetti L, and Beccari T, Origin of alpha-mannosidase activity in CSF. The international journal of biochemistry & cell biology 87 (2017) 34–37. [PubMed: 28359775]

[47]. Borgwardt L, Lund AM, and Dali CI, Alpha-mannosidosis - a review of genetic, clinical findings and options of treatment. Pediatric endocrinology reviews : PER 12 Suppl 1 (2014) 185–91. [PubMed: 25345101]

[48]. Borgwardt L, Dali CI, Fogh J, Mansson JE, Olsen KJ, Beck HC, Nielsen KG, Nielsen LH, Olsen SO, Riise Stensland HM, Nilssen O, Wibrand F, Thuesen AM, Pearl T, Haugsted U, Saftig P, Blanz J, Jones SA, Tylki-Szymanska A, Guffon-Fouiloux N, Beck M, and Lund AM, Enzyme replacement therapy for alpha-mannosidosis: 12 months follow-up of a single centre, randomised, multiple dose study. Journal of inherited metabolic disease 36 (2013) 1015–24. [PubMed: 23494656]

[49]. Roy S, Karmakar M, and Pearlman E, CD14 mediates Toll-like receptor 4 (TLR4) endocytosis and spleen tyrosine kinase (Syk) and interferon regulatory transcription factor 3 (IRF3) activation in epithelial cells and impairs neutrophil infiltration and Pseudomonas aeruginosa killing in vivo. J Biol Chem 289 (2014) 1174–82. [PubMed: 24275652]

[50]. Sharma L, Amick AK, Vasudevan S, Lee SW, Marion CR, Liu W, Brady V, Losier A, Bermejo SD, Britto CJ, Lee CG, Elias JA, and Dela Cruz CS, Regulation and Role of Chitotriosidase during Lung Infection with Klebsiella pneumoniae. J Immunol 201 (2018) 615–626. [PubMed: 29891554]

[51]. Tsukuba T, Yanagawa M, Kadowaki T, Takii R, Okamoto Y, Sakai E, Okamoto K, and Yamamoto K, Cathepsin E deficiency impairs autophagic proteolysis in macrophages. PloS one 8 (2013) e82415. [PubMed: 24340026]

[52]. Ray V, Anti-Psl monoclonal antibodies as novel immunotherapeutics against P.aeruignosa biofilms. ASM meeting abstract (2015).

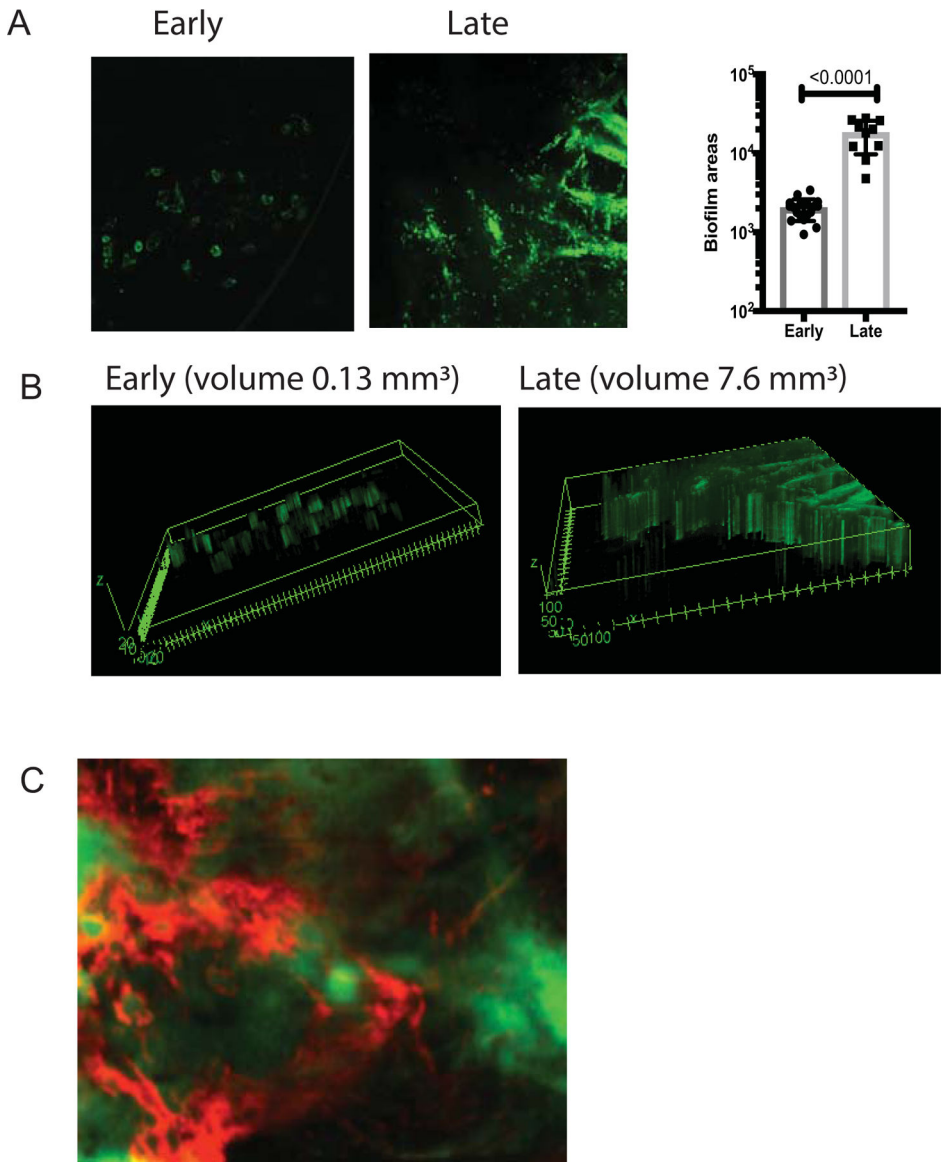

Figure 1. *P. aeruginosa* biofilms are surrounded by *psl*.

(**A**) C57BL6/N mice were infected with 1.10^5 cfu/eye *P. aeruginosa* PAO1 expressing CrdA-GFP. The intravital microscopy was carried out at early (12h) and late (24h) post-infectious challenge. Individual mice were imaged longitudinally. Areas covered with bacterial microcolonies or biofilms were calculated using Image J analysis. Each symbol represents individual bacterial cluster/microcolony. Student's *t*-test. (**B**) 3D-reconstructions of early and late bacterial biofilms. Volumes of biofilms per image were shown for comparison. (**C**) Biofilms were stained with fluorescently labeled anti-Psl mAb Cam003 (red) which was applied topically 15 min before imaging. Images were recorded at 40x. Psl (red) staining was adjacent or co-localized to *P. aeruginosa* (green). All images are representative of five individual experiments with 1–2 imaged mice per experiment. Imaging across central cornea revealed that bacterial microaggregates were seen during early hours of infection, whereas bacterial biofilms were formed as infection progressed. *P. aeruginosa* PAO1 CdrA-GFP

(green) clusters were surrounded by red Psl-stained polysaccharide, consistent with the definition of a biofilm.

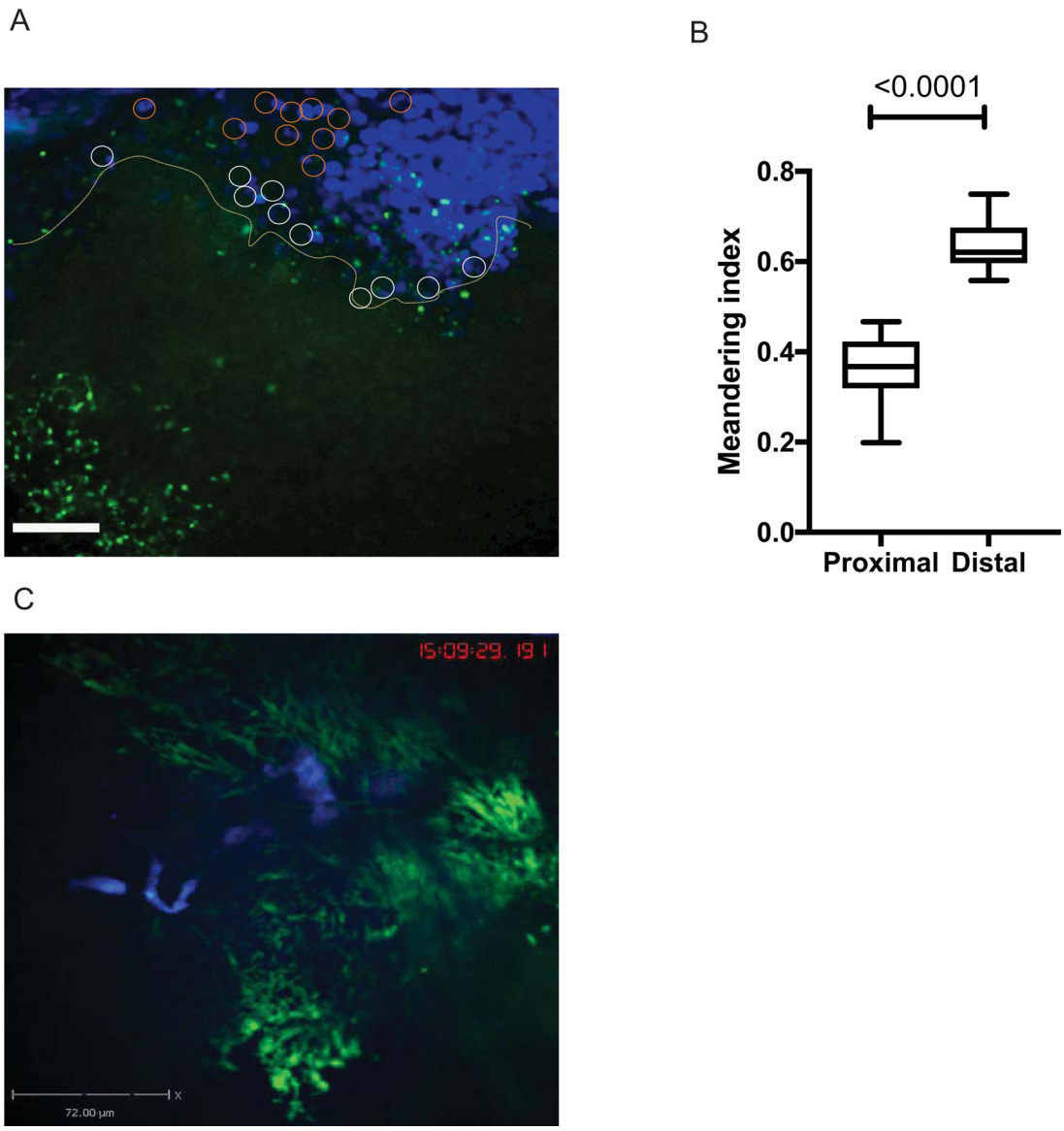

Figure 2. Neutrophils do not penetrate bacterial biofilms.

C57BL6/N mouse was infected with 1×10^5 cfu/eye PAO1-GFP. Mice were given fluorescent anti-Ly6G-Alexa 647 IV to label neutrophils. (**A**) Neutrophil swamps were migrating towards bacterial biofilms (green). Still image from S1. Bar size 72 µm. (**B**) Meandering indexes were calculated using MatLab and plotted. Neutrophil motilities differed depending on whether neutrophils appeared proximal to the biofilm (white circles) or distal (orange circles). Proximally located PMNs had significantly lower motilities when compared to the ones within the swamps or at a distance where bacteria were planktonic. Student's *t*-test. S1 movie is representative of three independent experiments. (**C**) Crawling neutrophils (blue) probe the bacterial clusters (green) (Still image from S2). *P. aeruginosa* PAO1 appear green, less mobile, and individual bacterial cells visibly move back and forth demonstrating restricted mobility within microcolonies. The movie displays crawling neutrophils that probe

bacterial microcolonies, but do not enter them. The movie is representative of more than three independent experiments. Video recording, 50 min.

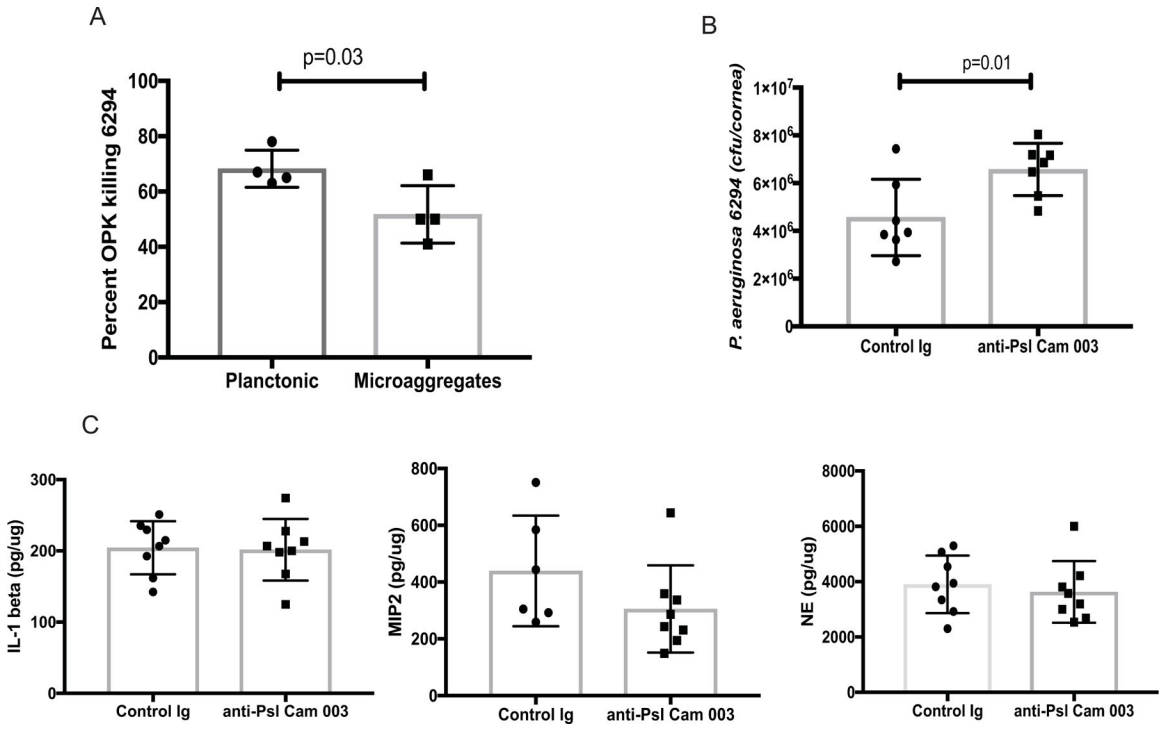

Figure 3. Topical application of anti-*psl* MAb Cam003 is not protective.

(A) Percent OPK of *P. aeruginosa* 6294 grown in a planktonic and microaggregate form. The anti-Psl mAb Cam003 shows significant opsonophagocytic killing against 6294, which is decreased when bacteria are allowed to form microaggregates *in vitro*. Student's *t*-test. **(B)** Topical application of 400 μg of Cam 003 onto infected eyes does not improve bacterial clearance. The mAb-treated eyes show a twofold increase in bacterial presence. Student's *t*-test. p=0.01. Data are representative of three independent experiments. **(C)** No significant differences in tissue IL-1β, MIP-2, and NE levels among Cam 003-treated and control Ab-treated mice. Student's *t*-test. Each symbol represents individual animals.

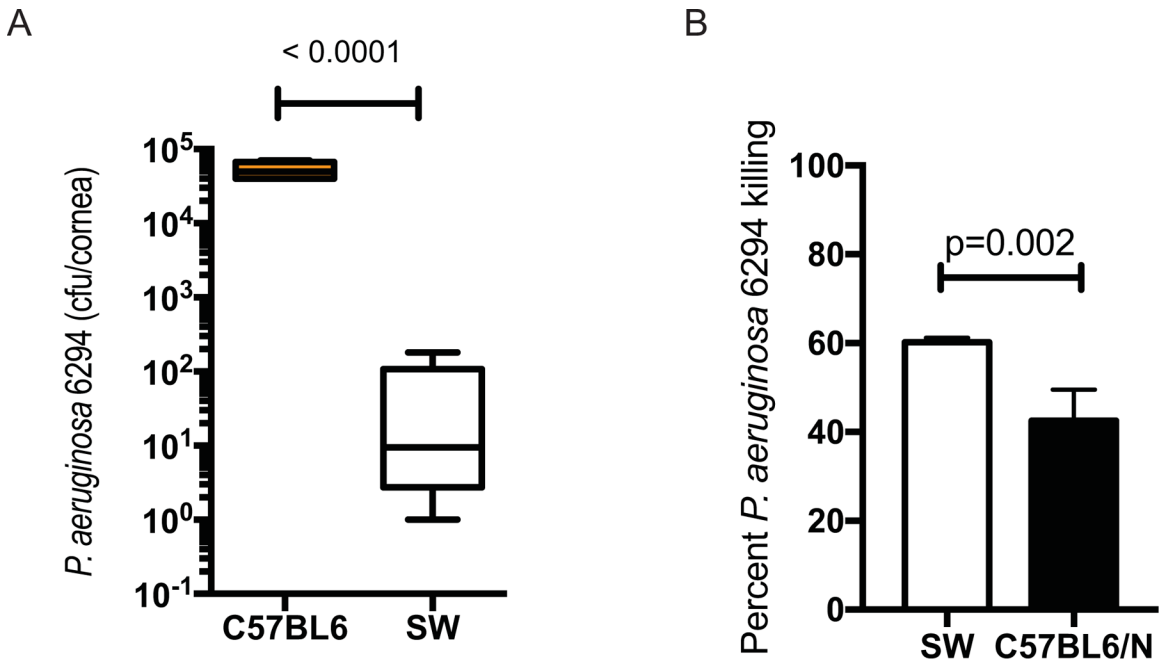

Figure 4. SW mice are resistant to *P. aeruginosa* 6294–induced keratitis.

(A) Cohorts of SW (N=9) and C57BL/6 (N=5) mice were infected with 1×10^6 cfu of *P. aeruginosa* 6294 and bacterial burdens in the cornea quantified at 48h after the onset of infection. Student's *t*-test. Experiments were repeated trice. **(B)** SW-derived PMNs kill *P. aeruginosa* 6294 more efficiently than C57BL6/N-derived PMNs. Mature neutrophils were purified from bone marrow of SW and C57BL/6N mice (Stem Cell), and exposed to 6294 at MOI 1 for 90 min as in [28; 52]. Aliquots from the reactions were plated. Student's *t*-test. Data are representative of two independent experiments.

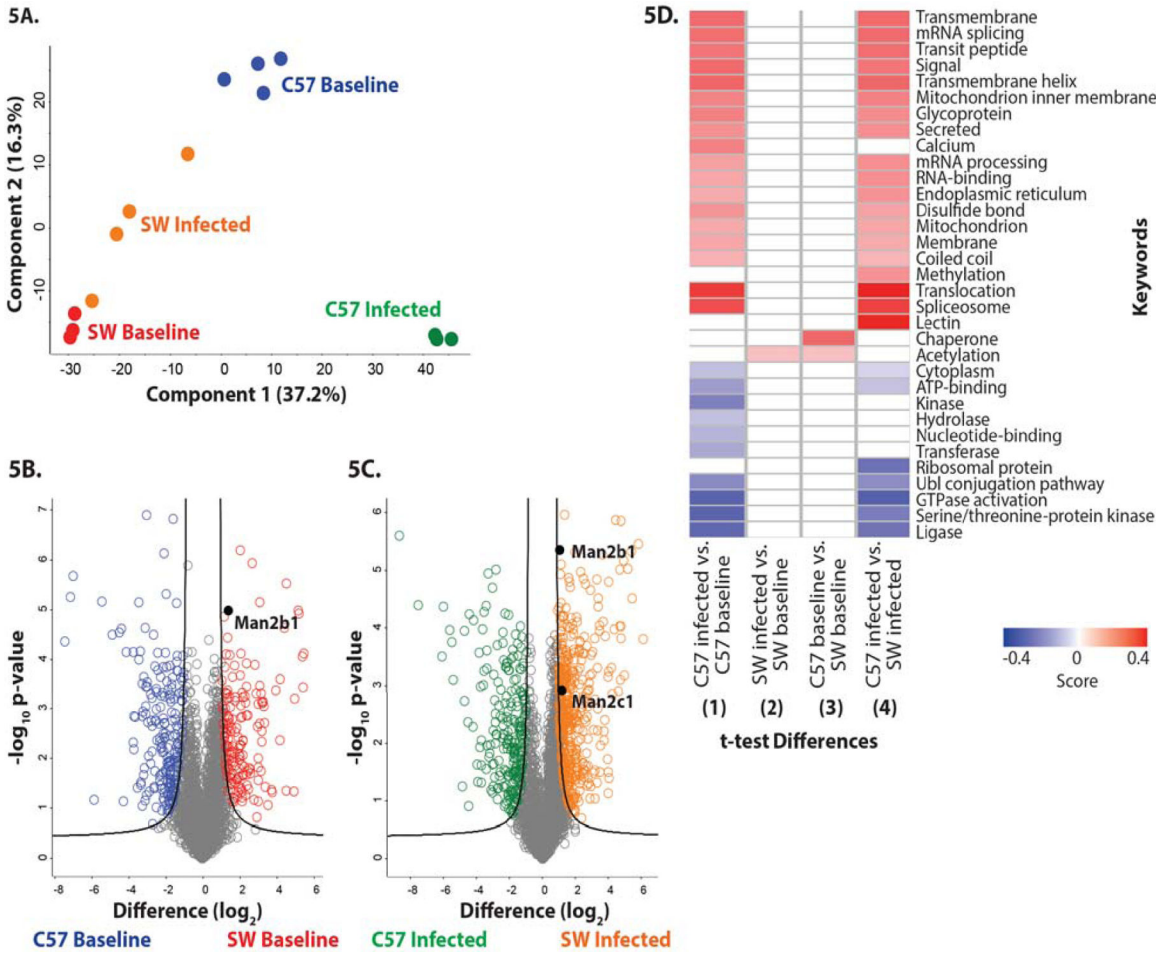

Figure 5. Differential protein abundance in SW and C57BL6/N-derived neutrophils from baseline and *P. aeruginosa*-infected mice.

(A) Principle component analysis representing the proteomes of samples harvested from neutrophils derived from non-infected SW (red) and C57BL/6 mice (blue), and infected SW (orange) and C57BL/6 (green) mice. Experiment was performed with a minimum of biological triplicates and measured on the mass spectrometer in two independent experiments. **(B)** Volcano plot depicting all identified proteins in neutrophils harvested from non-infected SW and C57BL/6 mice. The significantly different proteins with an increase in abundance at baseline in SW mice are shown in red, whereas those in the C57BL6-derived neutrophils are shown in blue. Data are representative from two independent experiments performed in at least biological triplicate. A Welch's *t-test* was performed to determine significant differences in protein abundance ($p\text{-value} < 0.05$) using Benjamini-Hochberg FDR correction at 5%. The position of Man2b1 is highlighted. **(C)** Volcano plot depicting neutrophil proteomes from infected SW and C57BL/6 mice. The significantly different proteins with an increase in abundance during infection in SW mice are shown in orange, whereas those in the C57BL/6-derived neutrophils are shown in green. Data are representative from two independent experiments performed in at least biological triplicate. A Welch's *t-test* was performed to determine significant differences in protein abundance ($p\text{-value} < 0.05$) using Benjamini-Hochberg FDR correction at 5%. The position of Man2b1

and Man 2c1 are highlighted. **(D)** 1D annotation enrichment profile based on keywords for comparisons among baseline and infected SW and C57BL/6-derived neutrophil samples. Data are representative from two independent experiments performed in at least biological triplicate. A two-sample Student's *t-test* was performed (*p-value* < 0.05) using Benjamini-Hochberg FDR correction at 5% with scores between < −0.5 and < 0.5.

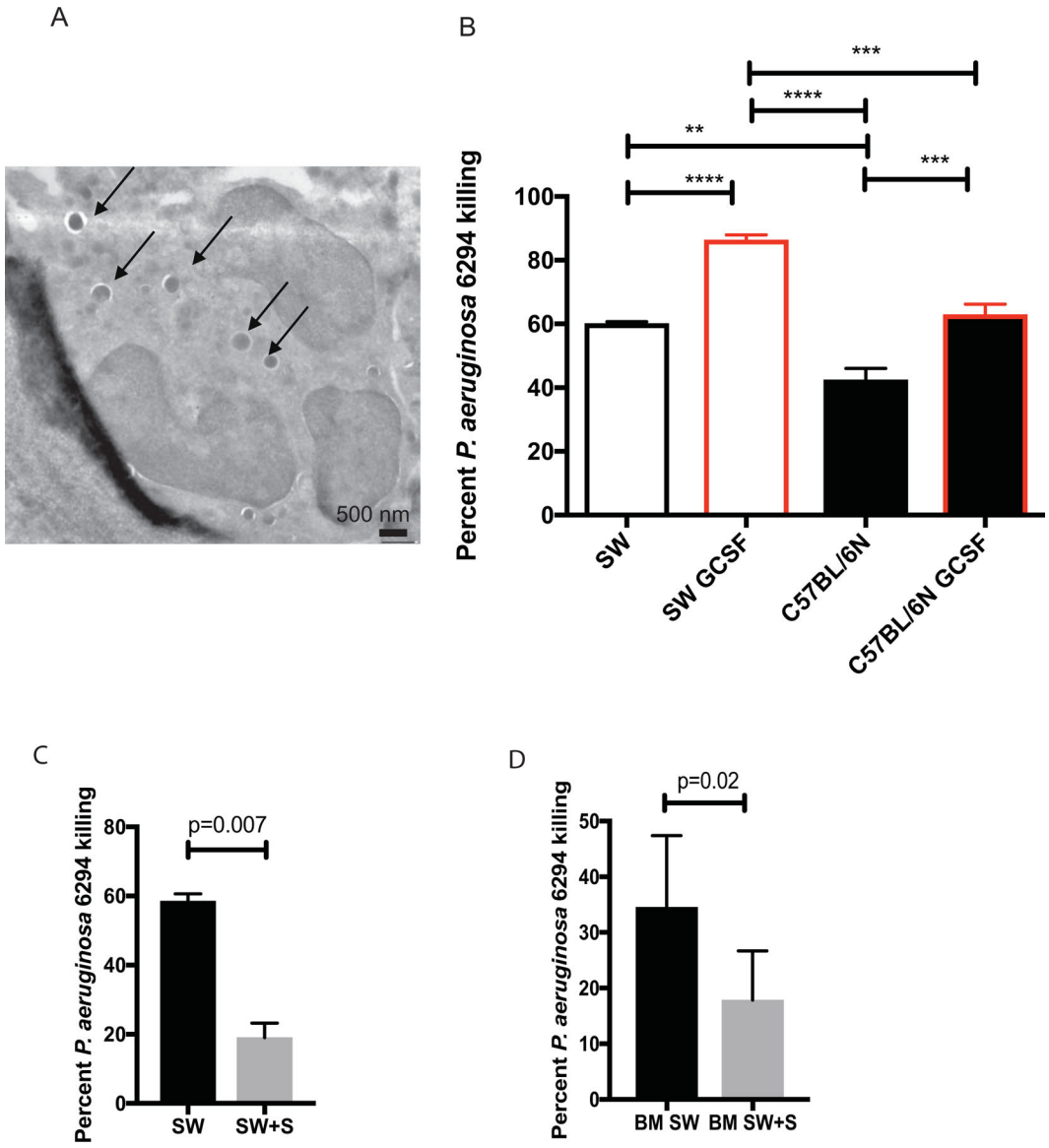

Figure 6. Swainsonine inhibits SW neutrophil bactericidal activities against *P. aeruginosa*.

(A) Electron micrograph image of SW-cell line derived PMNs phagocytosing *P. aeruginosa*. Individual bacterial cells engulfed by the PMN are shown with arrows. ***(B)*** *In vitro* generated SW and C57BL6/N neutrophils were primed with GCSF and exposed to *P. aeruginosa*. Percent bacterial killing was calculated. One-way ANOVA. Data demonstrate that SW-derived neutrophils retain superior bactericidal activity over C57BL/6N neutrophils. Data are representative from one out of four individual experiments. ***(C)*** *In vitro* generated, primed with GCSF SW neutrophils were exposed swainsonine (SW+S) or vehicle control (SW) and challenged with *P. aeruginosa* 6294. Percent bacterial killing was calculated. Student's *t*-test. Data are representative of two experiments. ***(D)*** Bone marrow-derived SW neutrophils were exposed to swainsonine and *P. aeruginosa*. Percent bacterial killing was calculated. Student's *t*-test.

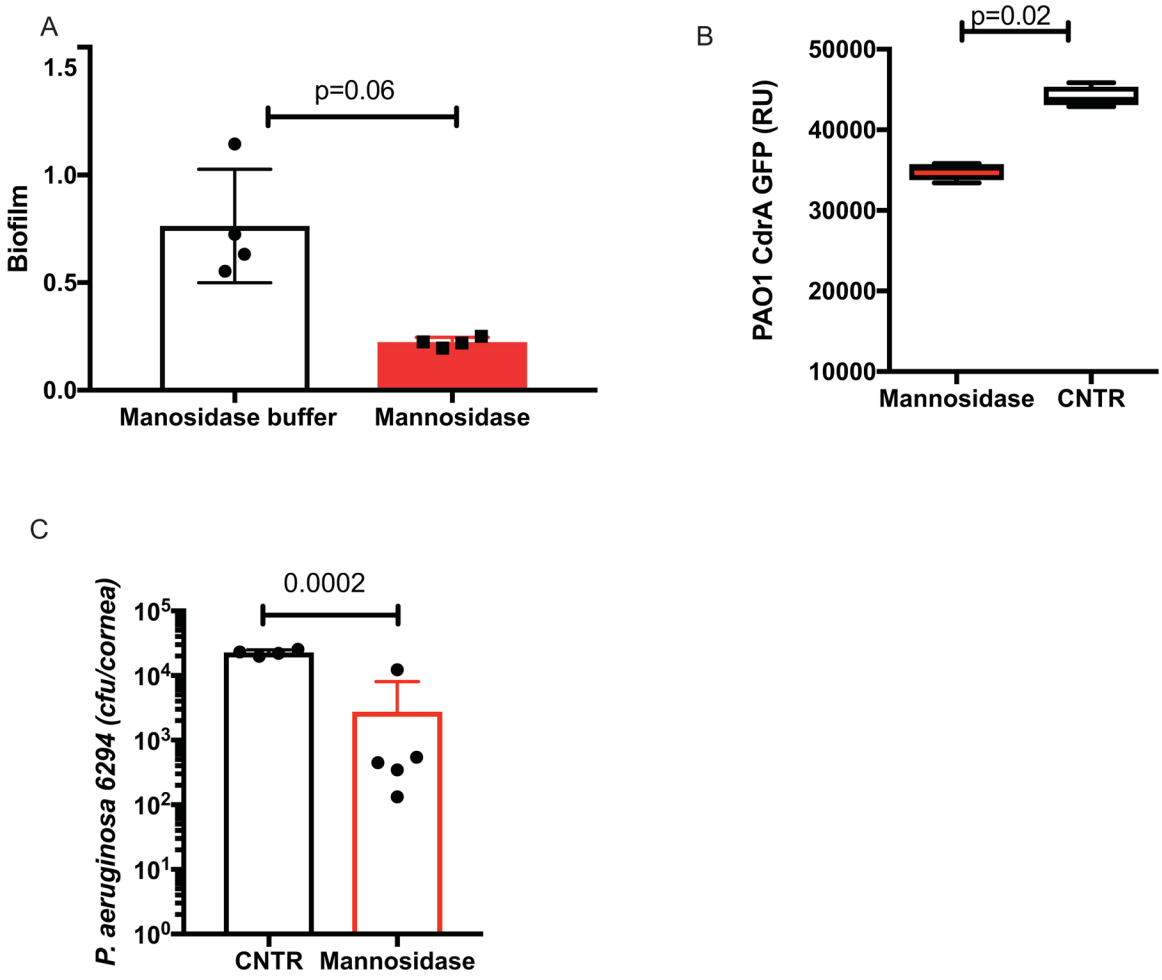

Figure 7. Alpha mannosidase treatment facilitates *P. aeruginosa* clearance in C57BL6/N mice.

(A) *P. aeruginosa* 6294 was allowed to form biofilms *in vitro* for 24 h and were exposed to 10U of α-mannosidase for 2 h at 37^0C. Bacterial biofilms stained and measured. Student's *t*-test. (p=0.006). Data are representative of two experiments. **(B)** *P. aeruginosa* PAO1-CrdA-GFP was allowed to form biofilms *in vitro* for 24 h and were exposed to 10U of alpha mannosidase for 2 h at 37^0C. Bacterial biofilms were washed, and fluorescent signal measured. Student's *t*-test. (p=0.05). Data are representative of two independent experiments. **(C)** C57BL/6N were infected with *P. aeruginosa* 6294 at 1.10^6 cfu/cornea, treated with 0.2 U/drop α-mannosidase four times daily, starting at 12h post the onset of infection. Student's *t*-test, (p=0.01). Data are representative of two independent experiments with 5 mice per group.